Solar Energy Materials and Solar Cells 185 (2018) 66–74

Contents lists available at ScienceDirect

Solar Energy Materials and Solar Cells

journal homepage: www.elsevier.com/locate/solmat

Lock-in thermography with depth resolution on silicon solar cells

O. Breitenstein[a,*], H. Straube[b], K. Iwig[c]

[a] Max Planck Institute of Microstructure Physics, Halle, Germany
[b] Jenoptik Optical Systems GmbH, Jena, Germany
[c] Dekra, Halle, Germany

ARTICLE INFO

Keywords:
Lock-in thermography
Solar cell characterization
Depth-dependent investigation
3D analysis

ABSTRACT

Lock-in thermography (LIT) is the standard method for imaging and evaluating leakage currents in solar cells. For usually applied lock-in frequencies in the order of 10 Hz, silicon solar cells are considered to be thermally thin. Hence, depth-dependent investigations, as they are performed in non-destructive testing and failure analysis of ICs, were not performed until now by LIT. In this contribution two special LIT investigation and evaluation methods are introduced, which have the potential to judge whether some recombination occurs at the top, in the middle, or at the bottom of a Si solar cell. Such investigations can be useful to evaluate e.g. metal-induced recombination or the influence of crystal defects in multicrystalline solar material on the emitter or backside recombination. The methods are tested at a cell containing a diamond scratch in the emitter and backside recombination at the Ag back contact.

1. Introduction

The technique of lock-in thermography (LIT), which is widely used in non-destructive evaluation (NDE) [1,2], is also established in solar cell research for imaging and quantitatively evaluating inhomogeneous dark currents in solar cells [3]. While the primary goal of LIT in NDE is to "look below the surface", hence to detect hidden irregularities [2] and to estimate their depth below the surface [4], LIT investigations of solar cells and modules is used for imaging local heat sources. Until now such investigations have been evaluated only two-dimensionally. The reason is that, at the usual lock-in frequencies between 3 and 30 Hz, solar cells are considered as "thermally thin" [3]. This means that their thickness of typically 180 μm is small compared to the so-called thermal diffusion length, which is about 1.7 mm for silicon at 10 Hz [3]. Therefore the thermal waves cross the material vertically nearly undamped, and the LIT image of a heat source at the front of a cell equals that of a heat source at its backside. This is not strictly the case, in particular when examining the temperature distribution close to a point source or sharp edge of the heat source, see [5].

It would be interesting to check also in solar cells whether a local heat source is located at the top (close to the emitter), in the middle (in the bulk), or at the bottom of a cell (at the back contact). As a rule, the recombination in the free emitter (outside of the metallization) or at the back contact is assumed to be homogeneous. However, there are indications obtained by CELLO [6] that the back contact recombination velocity in multicrystalline (mc) solar cells is inhomogeneous, and dark lock-in thermography (DLIT) investigations have indicated that also the recombination in the metallized emitter of mc cells may depend on the bulk lifetime [7]. For cross-checking these results, LIT investigations with depth resolution would be desirable.

Also in failure analysis of integrated circuits LIT is used for detecting the depth position of faults causing local heat sources [8]. In this so-called "3D analysis" the measurement of the phase of the LIT signal for various lock-in frequencies allows one to determine the depth of the heat source below the surface. This investigation, however, is not performed on massive silicon material but on stacks of several thin dies (chips) glued together. Here the glue layers between the dies lead to a measurable and frequency-dependent phase shift if the thermal wave travels from die to die, which is evaluated. Moreover, in these investigations the heat sources can be assumed to be point-like, hence their geometry is known. This is not the case for the investigation of solar cells, where the local heat sources (recombination sites) have an irregular and generally unknown geometry. It will be demonstrated in the following section that this source geometry strongly influences the local phase of the thermal waves much stronger than the depth position. Therefore, and since the depth-dependent phase differences are much smaller in solar cells than in stacked ICs, the previous 3D evaluation method [8] cannot be applied here.

In the following section the physical problem to be solved is described in more detail and the simulation and evaluation methods are introduced. Then in Sect. 3 two different methods will be introduced that may allow to check whether a local heat source is at the top, in the

* Corresponding author.
E-mail address: breiten@mpi-halle.mpg.de (O. Breitenstein).

https://doi.org/10.1016/j.solmat.2018.05.009
Received 5 April 2018; Received in revised form 2 May 2018; Accepted 4 May 2018
0927-0248/ © 2018 Elsevier B.V. All rights reserved.

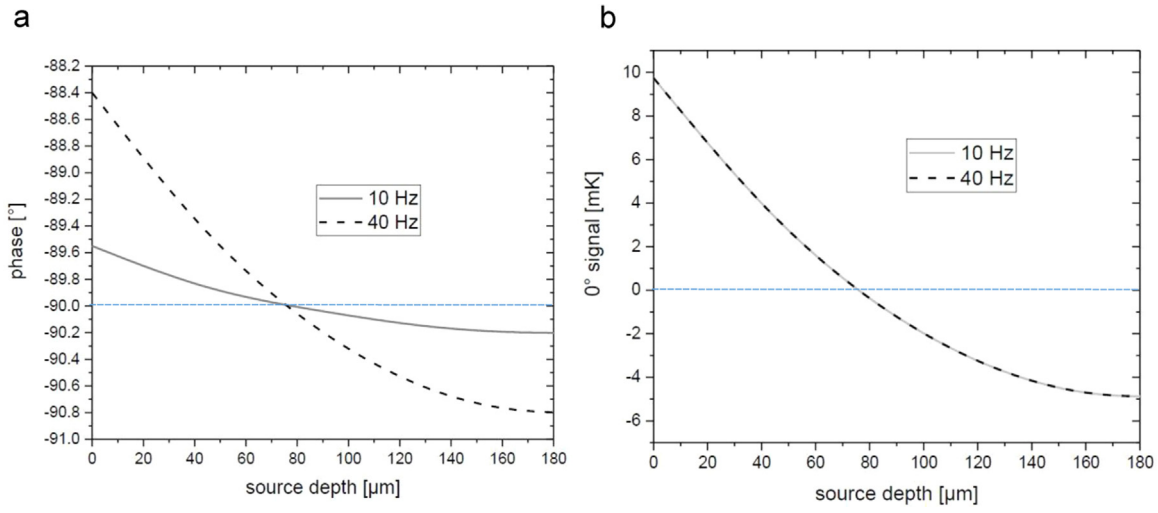

Fig. 1. (a) Phase signal and (b) 0° (in-phase) signal of a homogeneous heat source (1 mW/pixel) at 10 and 40 Hz as function of source depth in a 180 µm thick Si substrate.

middle (hence in the bulk), or at the bottom of a solar cell. These methods will be verified by simulations. In Sect. 4 these methods are tested on a solar cell containing a scratch at the top and preferred recombination at the Ag contact at the bottom. The results will be discussed in Sect. 5.

2. Simulation and evaluation methods and results

Deconvolution of LIT images can be used to deduce the power density distribution of the sample under investigation [3]. This task was performed here using DECONV [9]. This tool can perform two tasks: (1) It can simulate LIT images for a given pulsed power density distribution by performing a spatial convolution. (2) It can be used to evaluate given (experimental or previously simulated) LIT images by performing a spatial deconvolution, leading to the power density distribution that was responsible for the LIT images. The point spread functions (PSFs) necessary for the convolution and deconvolution are generated by DECONV for different sample geometries and lock-in frequencies, based on the formalism and specific functions developed in [5]. Possible source geometries are thermally thin samples, thermally thick samples, samples with a finite thickness, and finite and infinite thick samples with a highly conducting layer (HCL) on top. The latter option was developed for evaluating thin film silicon solar modules on glass [5]. The substrate thickness, the depth of the heat source below the surface, and the observation depth (where the temperature- (T-) modulation is detected; e.g. at the top or at the bottom) can be chosen, but all heat sources are assumed lying in one plane at the same depth. The substrate and HCL properties (thermal conductivity, density, specific heat capacity), the pixel size, and the lock-in frequency can be chosen.

DECONV allows to perform deconvolutions by an iterative and, what is used in this contribution, by the fast Fourier transform (fft) method using the Wiener filter, see e.g. [3]. The fft method generally works in complex number space. First, the software converts the DLIT images and PSFs in real space $T(x,y)$ and $PSF(x,y)$ into their Fourier transforms in frequency space $t(u,v)$ and $psf(u,v)$. For these Fourier transforms a convolution is a simple multiplication and a deconvolution, leading to the Fourier transform of the power distribution $p(u,v)$, is a division. In the presence of noise, the Wiener filter method replaces this division by:

$$p(u,v) = \frac{psf^*(u,v)\,t(u,v)}{|psf(u,v)|^2 + K} \quad (1)$$

Here $psf^*(u,v)$ is the complex conjugate of $psf(u,v)$. For $K = 0$ this is equivalent to $p(u,v) = t(u,v)/psf(u,v)$. From $p(u,v)$ the power distribution in real space $P(x,y)$ is obtained by performing an inverse Fourier transform. Note that the parameter K defines the "degree of deconvolution". For increasing K the resulting power distribution appears increasingly blurred, but noise is increasingly suppressed. $K = 0$ means maximum possible deconvolution being accurate up to one pixel. In the presence of noise this setting leads to meaningless results. Since in the simulations in Sect. 3.2 no noise was considered, they were performed using $K = 0$, but for evaluating experimental images as a rule a finite K parameter has to be chosen.

The fft deconvolution can be performed in DECONV either in scalar mode, here only one LIT image is evaluated, or in complex mode. In the latter case two LIT images are evaluated at the same time. The in-phase (0°) LIT image is used as the real and the − 90° LIT image as the imaginary input. This deconvolution mode is considered as the most accurate one and outputs in DECONV a real result (which is the wanted power density distribution) and an imaginary result, which should be zero for all pixels since power density is not out of phase with the excitation of the sample in LIT.

Using the PSF as well as convolution and deconvolution fully describes the physical problem including the depth dependence. The most obvious way to extract the depth information from a heat source below the surface is to measure the phase of the temperature modulation at the surface, as it was done in [8]. For a thermal wave leaving a heat source, the phase reduces by 2π (= 360°) over a distance of 2π thermal diffusion lengths [3]. In silicon this would correspond for a wafer thickness of 180 µm and a lock-in frequency of 10 Hz (leading to a thermal diffusion length of 1.76 mm [3]) to a phase shift of 5.9°, which should be easily measurable. However, this holds only if the thermal wave travels in an extended body, as it is the case e.g. for horizontally travelling thermal waves in a solar cell. If we consider vertically travelling thermal waves in a wafer being thin compared to the thermal diffusion length, the thermal waves are multiply reflected at the surfaces and the resulting temperature modulation at the surface is a superposition of many thermal waves. This effect reduces the phase contrast between heat sources lying at the bottom and at the top of a wafer, which can be modeled using the PSF of a small but finite thickness sample (implemented in DECONV), where the heat sources can be assumed to lie at an arbitrary depth. Fig. 1(a) shows the result of this simulation performed for 10 and 40 Hz for a homogeneous heat source as a function of the source depth in a 180 µm thick substrate. Let us start by examining the phase signal. It is slightly above − 90° for depth zero and drops to below − 90° for increasing source depths. We see that the dependencies are non-linear and for 10 Hz the maximum phase difference is only 0.6°, but for 40 Hz it is 2.39°, which should be

measurable.

Note that the accurate measurement of the phase of the surface temperature modulation in a LIT experiment is not a trivial task. According to the experiences of the authors, all LIT systems show by nature a certain systematic phase error, which comes from the inevitable processing time for the images to be correlated, see [3]. As described there, the phase measurement assumes that the first image to be correlated in a lock-in period is taken exactly in the moment of the low-high-edge of the excitation trigger. This means that this trigger has to appear in the middle of the frame integration time of the first images used for correlation in a lock-in period. In reality this is hard to realize, leading to a certain systematic phase error of usual LIT systems. If absolute phase values have to be measured, as e.g. for 3D measurements on integrated circuits [8], this phase error must be compensated e.g. by measuring a test object showing a well-defined phase of the temperature modulation as described in [3].

Another source of a systematic phase error is the paint to be used in the following for ensuring that only the temperature modulation at the surface is measured. This paint has a relatively low thermal conductivity, maybe comparable to plastic materials. Even if it is used as a thin layer, it cannot always be considered as thermally thin, hence to show a thermal diffusion length being small compared to its thickness. Assuming that this paint has thermal properties close to e.g. PVC, the thermal diffusion length in this material at 40 Hz is about 37 µm, which is not small compared to the paint layer thickness of 10 … 20 µm. Hence, this paint layer may lead to a distinct phase shift of the detected IR radiation if thermal waves travel through.

A second LIT signal, which is useful for depth-dependent investigations, is the 0° (in-phase) signal. As the simulations for 10 and 40 Hz for extended heat sources have shown, the − 90° and the amplitude signal vary by less than 0.1% for different source depths, hence these signals are not appropriate for performing depth resolution. The 0° signal, however, should be zero for an extended heat source in a thermally thin sample, hence for a sample of finite thickness it may be a measure of the source depth. Indeed, Fig. 1(b) shows results of this simulation for an extended heat source and a pixel size of 156 µm (corresponding to 512 × 512 pixels for an imaged field of 80 × 80 mm) and 1 mW/pixel, assuming a silicon substrate of 180 µm thickness, for source depths varying between 0 and 180 µm at lock-in frequencies of 10 and 40 Hz. We see that the 0° signal is positive for the source lying at the surface and becomes negative for higher source depths. Interestingly, the 0° signals for 10 and 40 Hz are exactly the same, but the − 90° signals are not (1404 mK for 10 Hz and 351 mK for 40 Hz, independent of source depth). Also this dependence is non-linear with slope zero for the source at the bottom of the substrate (180 µm). Note that a surface can be described by virtual mirror heat sources outside of the device, leading to zero heat flow across the surface, see [3]. Hence, if the heat source approaches the back surface, a second virtual heat source approaches the back surface from outside, leading to a nearly depth-independent action of both sources. This simulation shows that, for a homogeneously distributed heat source, the depths position of the source in this device should be measurable by monitoring the phase or the 0° signal. A high frequency should be preferred, since here the phase contrast and the 0°/− 90° signal ratio is largest. It is obvious that depth-dependent effects can be studied best if the ratio thermal diffusion length to wafer thickness is largest.

Unfortunately, in a solar cell the local heat sources (recombination sites or shunts) represent no homogeneous heat source and their magnitudes and shapes are generally unknown. The phase of the T-modulation in source position strongly depends on the source geometry [3]. Moreover, different heat sources lying at the top, in the middle, or at the bottom of a solar cell may be located at the same lateral position, hence they may overlap. In order to test possible approaches for depth information extraction in a simulation, a model solar cell with heat source distributions shown in Fig. 2(a–c) was constructed, which contains different, partly overlapping, heat sources at the top, in the middle and at the bottom of the 180 µm thick model cell. The pixel size is again 156 µm. For checking the influence of different source geometries, the patterns contain lines with two different widths. From these patterns as heat source distributions, with a power density of 1 mW/pixel for all white regions in the given source depth, 0° and − 90° images were simulated in DECONV, and the data of all three simulated 0° and all three − 90° images were added up, leading to 0° and − 90° LIT results of the 3-dimensional model solar cell containing all these power distributions in different depths. These simulations have been performed at 10 and 40 Hz frequency, here we show only results for 40 Hz. Fig. 2(d) shows the resulting amplitude image, (e) shows the 0° image, and (f) shows the phase image. The artifacts in the phase image outside of the heat sources are keel over effects, since the displayed phase starts again at 0° if it is lower than − 360°. The same images have been simulated also for backside inspection (observation depth 180 µm), but there are no visible differences to the images seen in Fig. 2(d–f).

The amplitude image Fig. 2(d) appears as usual as a blurred sum of all power distributions. The strongest amplitude signal appears in the middle of the cross at the right, where the heat sources at the top, in the middle, and at the bottom of the wafer overlap. The 0° image (e) shows a better spatial resolution and overshoots into the negative outside of the heat sources, also as usual, see [3]. Moreover, in this image the thinner stripes show a stronger signal than the wide ones. Also in the phase image (f) we see that the thinner stripes show a higher (less negative) phase signal than the wider ones. This is both due to the well-known fact that, for a line source in a thermally thin device, a phase signal in source position of − 45° is expected, but for an extended power source of − 90° [3]. Note that neither in the phase image nor in the 0° image heat sources of different depth can be distinguished from each other visually.

3. Methods for depth-resolved imaging

3.1. The front-minus-back difference method

It was mentioned above that all simulated images for front and backside imaging appear visually identical. However, there are small differences, which can be made visible by calculating the corresponding front-minus-back difference images. Fig. 3 shows these images for the 0° (a), the phase (b), and the amplitude images (c). Actual measurement of this kind is possible and is demonstrated below.

In all images in Fig. 3 the heat sources in the middle of the wafer remain invisible. This could be expected since such heat sources produce the same T-modulation at the front and at the backside. In all cases the heat sources lying at the top of the wafer appear with positive (bright) and that at the bottom with negative (dark) contrast. Interestingly, all these images are not significantly blurred, though the input images seen in Fig. 2 are. Obviously, the local T-modulation at the surface can be split into one contribution due to horizontal heat diffusion, which appears blurred, and one due to vertical heat diffusion, which appears un-blurred, at least if the pixel size is not small compared to the wafer depth. The different physical properties of horizontally and vertically travelling thermal waves in wafers have been discussed already in Sect. 2.

The most interesting image is the 0° difference image Fig. 3(a). As shown in the last section, the 0° image is positive for homogeneous heat sources lying at the top and negative for sources lying at the bottom. Hence, for such sources the difference signal is not small compared to the average 0° signal. However, for inhomogeneous heat sources the inhomogeneity-caused 0° signal is large compared to the depth-dependent 0° signal, note the a factor of 10 different scaling ranges between Fig. 2(e) (−141 to 249 mK) and Fig. 3(a) (−14.7 to 14.7 mK). In the 0° difference image Fig. 3(a) the brightness of the imaged heat sources is independent of the source geometry (stripe width), in contrast to the input image seen in Fig. 2(b). The 0° difference image Fig. 3(a) is also strictly additive, hence overlap with the heat source in

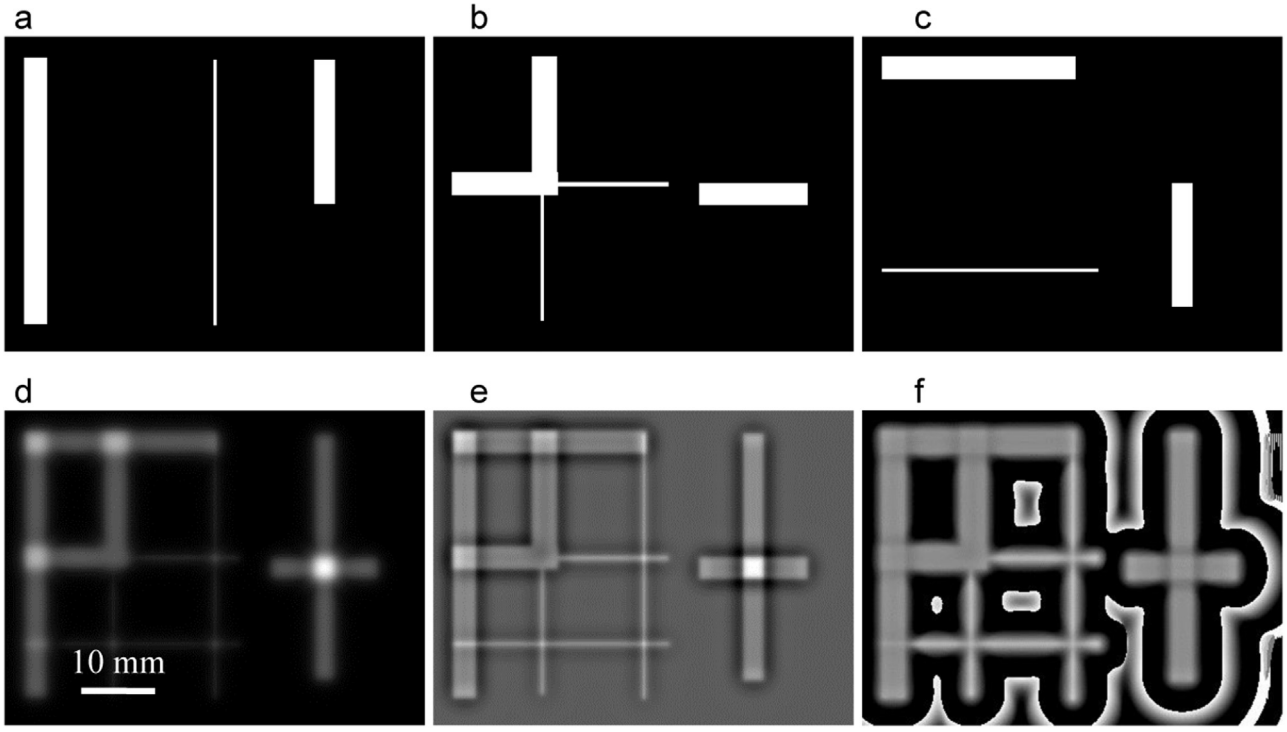

Fig. 2. (a) Assumed power distribution at the top, (b) assumed power distribution at the middle, (c) assumed power distribution at the bottom, all 1 mW/pixel, (d) simulated amplitude image (0–1097 mK), (e) 0° image (− 141 to 249 mK), and (f) phase images (− 180 to 0°) of the model solar cell.

the middle of the wafer depth (Fig. 2b) does not influence the difference result, and overlap of front and backside heat sources of the same magnitude leads to zero signal (good visible in the upper left corner). Hence this image allows to measure the power density of a heat source if it is lying at the top or at the bottom of the wafer, see below.

The simulated − 90° difference image (not shown) looks identical to the 0° difference image but shows a significantly lower magnitude of ± 1 mK. Due to the dramatically lower dynamic range (amplitude of difference image compared to the raw images), the use of these images to extract depth information is limited.

Both phase and amplitude difference images Fig. 3(b) and (c) look qualitatively similar to the 0° difference image (a), but here we see an influence if the heat source in the middle of the depth overlaps with the top or bottom heat source, and the brightness depends on the width of the stripes. These differences are obviously caused by the fact that both the phase and the amplitude image are non-linear results of the 0° and the − 90° images; only the latter have the property to superimpose linearly. Although the amplitude difference image looks similar to the phase difference image, it shares the property of low dynamic range with the − 90° difference image and is therefore not useful for depth information extraction.

A possible advantage of the phase difference signal as compared to the 0° difference signal is that it is independent of the local power density of the heat sources. This is not visible in these simulations since here all heat sources show the same power density of 1 mW/pixel. However, it is well-known that all phase images are independent of the magnitude of the imaged heat sources, if the LIT signals of different heat sources do not overlap [3]. This means that, at least for a dominating local heat source, the phase difference image should allow a direct reading of the vertical position, independent of its power density. It can also be expected that the phase difference image reacts less sensitively to any differences of the IR emissivity between front and backside inspection. An important experimental consideration is that this phase difference image is independent of the systematic phase error of the LIT system. This, however, works only under the condition that the paint-induced phase error mentioned in Sect. 2 is negligible or is exactly the same for the front and the backside. The disadvantages of using the phase difference image over the 0° difference image are the non-linearity in the presence of multiple sources and that it reverts to high noise (magnitude 0–360°) in the absence of signal.

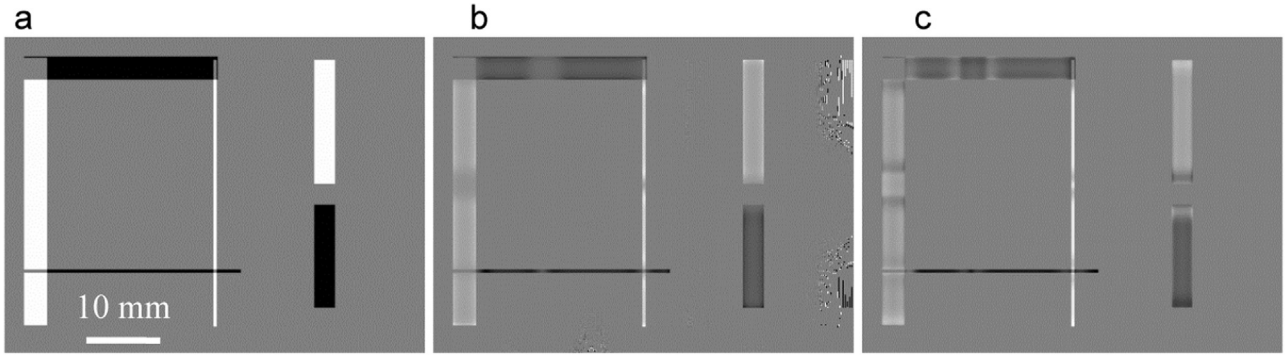

Fig. 3. Front-minus-back difference images of the 0° images (− 14.7 to 14.7 mK), the phase images (− 8.6 to 8.6°), and the amplitude images (− 11 to 11 mK).

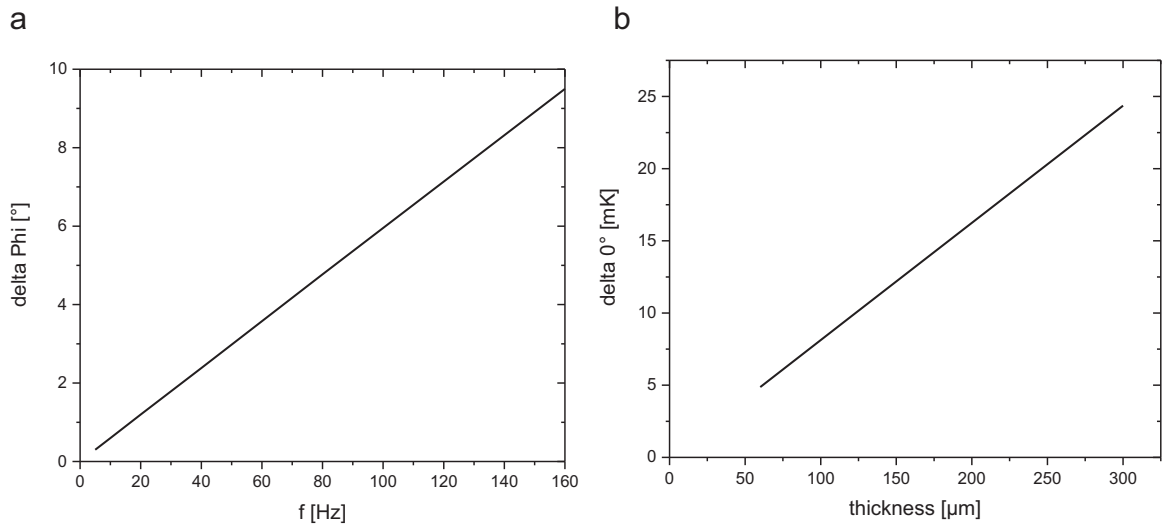

Fig. 4. (a) Phase difference signal for an extended heat source at the top and the bottom of a 180 µm thick wafer as function of frequency, (b) 0° difference signal as function of wafer thickness.

Fig. 4(a) shows the magnitude of the phase difference for an extended heat source lying at the top of a 180 µm thick wafer as a function of the lock-in frequency. This phase difference (which is proportional to $f_{\text{lock-in}}$ and equals 2.39° for an extended heat source at 40 Hz and 180 µm thickness) increases with the square of the wafer thickness, since it depends on the ratio of the wafer thickness to the thermal diffusion length, which decreases with $1/\sqrt{f_{\text{lock-in}}}$ [3]. Note that this phase difference is independent of the pixel size, but it depends on the source geometry and is larger for local than for extended heat sources. For a line source at 40 Hz and 180 µm thickness it is expected to be 10.59° and still 5.3° at 10 Hz. Hence, for line sources (e.g. scratches) the depth position could be measurable by the front-minus-back phase difference method, if there are no other phase errors.

It was shown above that the amount of the 0° difference signal is proportional to the local power density, if the heat source is lying either at the top or at the bottom of the cell. In this case this signal should be comparable to the local power density signal, as it comes out of the LIT image deconvolution performed e.g. by DECONV. Therefore another useful parameter is the ratio of the dissipated power density (in units of mW/pixel) for a heat source lying at the top to the magnitude of the 0° difference signal (in units of mK). This "0° difference scaling factor" (in units of mW/mK,pixel) allows to scale 0° difference images in units of mW/pixel, provided that the heat sources are lying at the top or at the bottom of the cell. According to Fig. 1(a) this scaling factor is independent of the lock-in frequency, but it depends on the wafer thickness. Fig. 4(b) shows the dependence of the 0° signal difference for 1 mW/pixel as a function of the wafer thickness. Also this dependence is linear. The 0° difference scaling factor is the inverse of this magnitude. For a 180 µm thick wafer the 0° difference signal is 14.62 mK leading to a scaling factor of 0.0684 mW/mK,pixel. This scaling factor can easily be converted to the scaling factor in units of mW/mK,cm^2 by dividing it by the pixel area. For a line source with 1 mW/pixel the calculated 0° difference signal in source position is 11.5 mK, slightly lower than that for an extended heat source. This small deviation is due to the fact that, for a pixel size of 156 µm at a wafer thickness of 180 µm, the pixel size is in the order of the wafer thickness. Hence, here the 0° difference image becomes already slightly blurred. If the heat source is lying at the backside of the wafer, both magnitudes in Fig. 4 become negative, see Fig. 3.

The application of this front-minus-back difference image method to measured DLIT images will be tested in Sect. 4. This difference image method should have the general advantage that it does not need any deconvolution procedure, since it works without significant blurring with the directly measured LIT image. On the other hand, it has the limitation that it needs LIT investigations from both sides of the device under exactly the same conditions, and the results have to be spatially aligned very exactly, which is experimentally more demanding.

3.2. The imaginary fft signal method

The main disadvantage of the method outlined in the preview section is the experimental complexity. Since the depth information of the source is present in the PSFs, it may be possible to extract this information from a single one-sided measurement. As mentioned in Sect. 2, the result of a fft deconvolution procedure is generally complex. An argument of the complex values other than zero for a given pixel has the physical interpretation of a heat source out of phase with the excitation. This can be excluded at common lock-in frequencies. Therefore, the only possible explanations for a deconvolution result with imaginary part are a wrong choice of PSF and imperfections in the measurement. The PSF is well known except for the depth information. Varying the depth parameter of the PSF until the imaginary part of the deconvolution vanishes should therefore be an option to extract the depth information from a given measurement. This use of the imaginary part of the deconvolution result as a check for the correctly chosen PSF was proposed already by Seidel et al. [4].

This is demonstrated in Fig. 5, displaying for simulated 0° and − 90° images of the model solar cell the real (a-c) and imaginary deconvolution results (d-f). Again, a wafer thickness of 180 µm and a frequency of 40 Hz was assumed. Since here previously simulated LIT images have been deconvoluted, which show no noise, the adjustment parameter K in Eq. (1) could be chosen as zero. We see that the real (power density) results under these three deconvolution conditions (a-c) are nearly identical. Only the sharp edges of the assumed heat sources appear slightly blurred, if a source depth lower than the real depth was assumed, and they show an overshoot if a depth larger than the real depth was assumed, which is good visible in Fig. 5(c). If for the evaluation of experimental images a certain deconvolution adjustment parameter K for limiting the noise is used, these overshoots (which anyway only appear on sharp edges of heat sources) will become invisible. Then the real (power density) images for all three assumed heat source depths will become identical. In the overlapping regions the power densities simply add up, as expected.

The imaginary results (d-f) clearly show whether the depth was correctly assumed or not. If the depth was correctly assumed, the imaginary signal is zero in these simulations. If it was assumed too low,

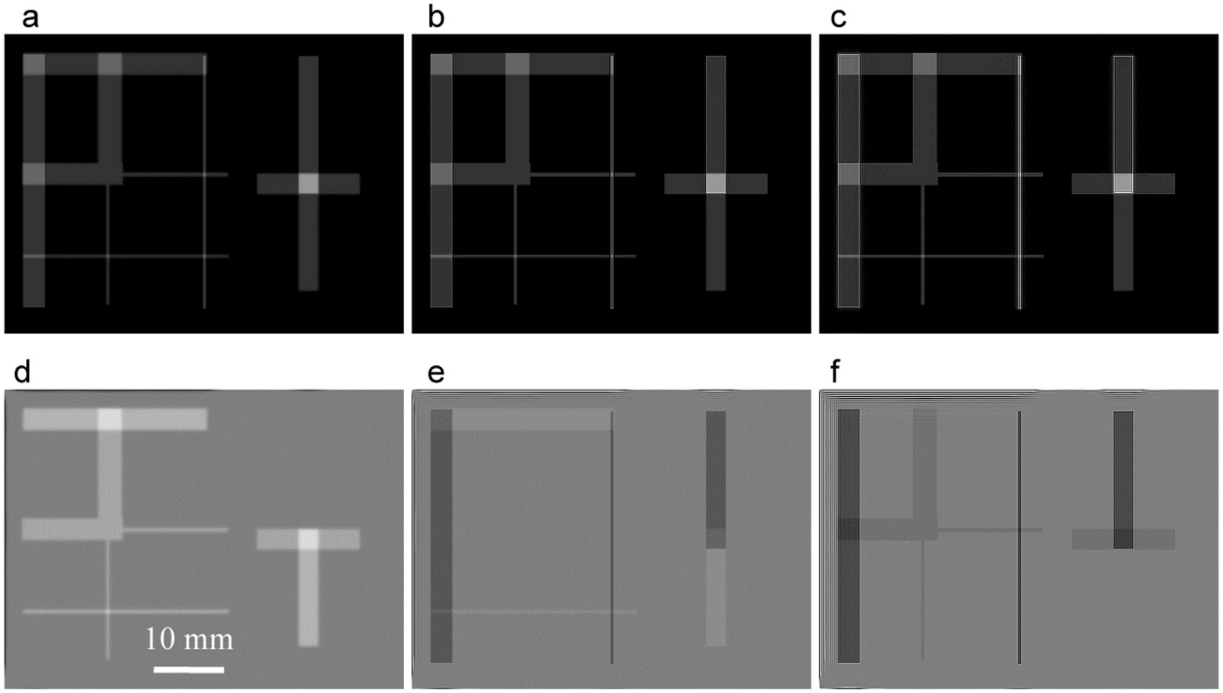

Fig. 5. Deconvoluted images (fft complex) assuming various source depths: (a) power, 0 μm, (b) power, 90 μm, (c) power, 180 μm, all scaled from 0 to 5 mW/pixel, (d) imaginary 0 μm, (e) imaginary 90 μm, (f) imaginary, 180 μm, all scaled from -10^{-4} to 10^{-4} a.u.

the imaginary signal is positive, and if it was assumed too high, it is negative. The imaginary results do not react linear to the depth error. For an assumed depth of 180 μm (Fig. 5f) the sources lying at 90 μm show less than half of the (negative) signal of the sources lying at the top ($-1.04*10^{-5}$ vs. $-4.16*10^{-5}$ a.u.). On the other hand, for an assumed depth of 0 μm (Fig. 5d) the sources lying at 90 μm show only a slightly lower brightness than that lying at 180 μm ($3.12*10^{-5}$ vs. $4.14*10^{-5}$ a.u.). If the middle depth of 90 μm was assumed (Fig. 5e), the sources lying above show a dark (negative, $-3.12*10^{-5}$ a.u.) and that lying below show a smaller bright (positive, $1.04*10^{-5}$ a.u.) imaginary signal. At least, the imaginary fft result describes the depth error monotonically and is zero for correctly assuming the depth. This property should remain also if a finite value of the adjustment parameter *K* is chosen.

The main advantage of this method, compared to the front-minus-back difference method introduced in Sect. 3.1, is that here only one LIT measurement taken at the top of the cell is necessary. Hence, there is no spatial alignment problem. A limitation is that this method needs the deconvolution procedure, which is known to degrade the signal-to-noise ratio. The practical application of this method in Sect. 4 will show whether this method is practicable or not.

4. Measurement results

Both methods were tested on a $156 \times 156\,mm^2$ sized industrial monocrystalline Al back surface field (BSF) standard technology cell showing two busbars. At the top of this cell a diamond scratch was made close to one busbar, leading to a line-shaped site of preferred recombination there. This cell contained 4 mm wide screen-printed silver stripes on the rear side in the positions of the busbars for soldering, which show a significantly larger backside recombination than the Al back contact. The scratch was made close to one busbar, leading to one heat source at the top (the scratch) and one at the bottom (the Ag stripe) in one image region. For measuring the cell from both sides, a 22 mm wide stripe at one edge of the cell containing this region was blackened at the top and at the bottom for ensuring that the LIT result reflects only the the T-modulation in these height positions. This has been done in this work by using the thermographic spray paint for standard applications by LabIR [10]. For obtaining an emissivity above 93% it is recommended to apply two layers of this paint, leading to a layer thickness of about 20 μm. We have found that, for performing lock-in thermography at a frequency as high as 40 Hz, the application of only one paint layer is more appropriate, since it leads to a lower paint-induced phase error as described in Sect. 2. Then the bottom LIT image must be horizontally mirrored and its position must be adjusted so that both images show the device pixel-accurate. Only then the front-minus-back difference can be calculated. This evaluation can only be successful if for the front and backside LIT measurement the power densities are the same (same local cell current), if emissivity is the same and close to unity for the front and back surface, and (at least for the 0° images) if the systematic phase error of the used LIT system is corrected.

DLIT images of the interesting cell region were made at a lock-in frequency of 40 Hz from the top and the bottom with an acquisition time of 2 h for each measurement by using the PV-LIT system of InfraTec GmbH Dresden [11]. The pixel size was 156 μm, the cell temperature was 25 °C and the cell current was about 6 A in both cases. Fig. 6(a) and (b) show the front-side phase and the 0° images for the blackened region of the cell containing the cell edge at the left, the scratch at the right, and the busbar at the top. Note that the about 2 mm wide stripe at the left is the region without Al contact at the bottom, which also shows an increased recombination activity. The phase image in Fig. 6(a) nicely shows the expected linear drop of the phase with increasing distance to the scratch and the slight overshoot at the edges of extended recombination regions, which were visible already in Fig. 2(f). While in the model cell of Fig. 2 there is no noise and the region outside of the model heat sources shows no heating, but in the real cell used for Fig. 6 we have a weak homogeneous heat dissipation outside of the preferred recombination sites. Therefore in Fig. 6(a) the phase signal returns for increasing distance to the scratch to −90° and shows a stronger noise, whereas in Fig. 2(f) it further reduces. As usual, the strongest phase noise is at the left of the image outside of the cell and at the top, where the IR signal is shadowed by the current rail. The measured 0° signal in Fig. 6(b) shows the expected undershoot outside

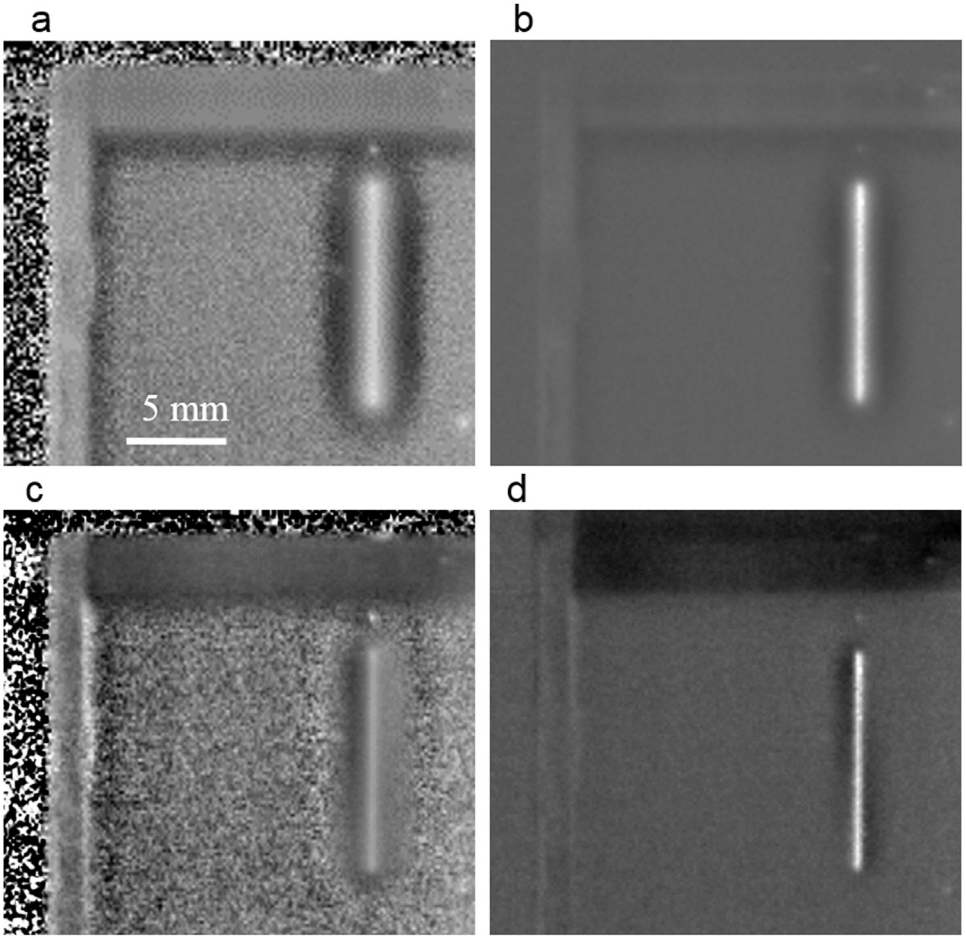

Fig. 6. (a) Front phase image of the scratch region (− 180 to 0°), (b) front 0° image (− 3 to 5 mK), (c) phase difference image (− 90 to 0°), (d) 0° difference image (− 1 to 2 mK).

of the scratch and the over- and undershoot at the edges of the homogeneous heating areas, which were visible already in Fig. 2(e).

The backside phase and 0° images were horizontally mirrored and subtracted from the front side images. This subtraction and the spatial alignment was performed by using the free and open source "GIMP 2" image manipulation software [12]. It turned out that the alignment procedure, which was performed in GIMP by moving one layer image on top of the other image in "subtract" mode, is very critical, since the two image positions may differ by less than one pixel. Therefore for this procedure the image size was up-sampled from 512 × 512 pixels to 2048 × 2048 pixels. Fig. 6(c) and (d) show the results of this procedure in the interesting region for the phase and the 0° images, respectively. We see that, as expected, the right scratch located at the top shows a quite sharp bright line in both images. The backside silver contact region at the top shows a dark contrast in (c) and (d), as expected. The 0° difference signal in the scratch region of Fig. 6(d) amounts to 1.33 mK. This corresponds with the scaling factor of 0.0684 mW/mK,pixel of Fig. 4(b) to a power density in this region of 90.9 μW/pixel. This roughly corresponds to the power density obtained in this region by LIT image deconvolution, as will be shown below. The residual error and also the residual blurr may be due to a different paint thickness in top and bottom, which may not only lead to a different phase but also to a different 0° signal reading. It must be said that the amount of the phase difference in Fig. 6(c) does not fit the value expected in Fig. 4(a). We believe that this is a result of the dissimilar phase error caused by the top and the bottom paint layer. Residual imperfections in these images will be discussed in Sect. 5.

Fig. 7 shows the results of the imaginary fft signal method by evaluating the LIT signals of the front side measurement. Here power and imaginary signal images for assuming the heat source to lie at the top and at the bottom are shown. The parameter K was chosen as 200, which significantly reduces the noise but causes only minor additional blur. We see that, as expected, the deconvoluted power density images do only weakly depend on whether the heat source was assumed to lie at the top (a) or at the bottom (b). However, the imaginary results (c) and (d), at least of the right scratch lying at the top, are dependent on this assumption. Here for the right scratch lying at the top the imaginary signal is noisy but on average close to zero if the height position was correctly assumed (c), and it is clearly negative if the position was assumed at the bottom (d). This corresponds to the simulation results shown in Fig. 5(f). Note that these results depend strongly on the correct choice of the systematic phase error correction. If the phase shows a systematic offset, the imaginary signal in source position may be positive or negative, depending on the sign of the phase error. Fortunately, DECONV contains the option to correct systematic phase errors. Here the phase error was chosen to minimize the imaginary deconvolution result for the scratch, if its height position was assumed correctly.

In Fig. 7 in the left two images (a and c) the depth of the scratch was correctly assumed (to be at the top) and in the right two images (b and d) wrongly (to be at the bottom), but that of the Ag back contact was correctly assumed. Indeed, the deconvoluted power distribution of the scratch in (a) appears sharper than that in (b), the latter also showing a stronger undershoot outside of the scratch. This indicates that, for describing the scratch, the PSF used for image (a) was more realistic than that used for (b), what was indicated already by the imaginary signal.

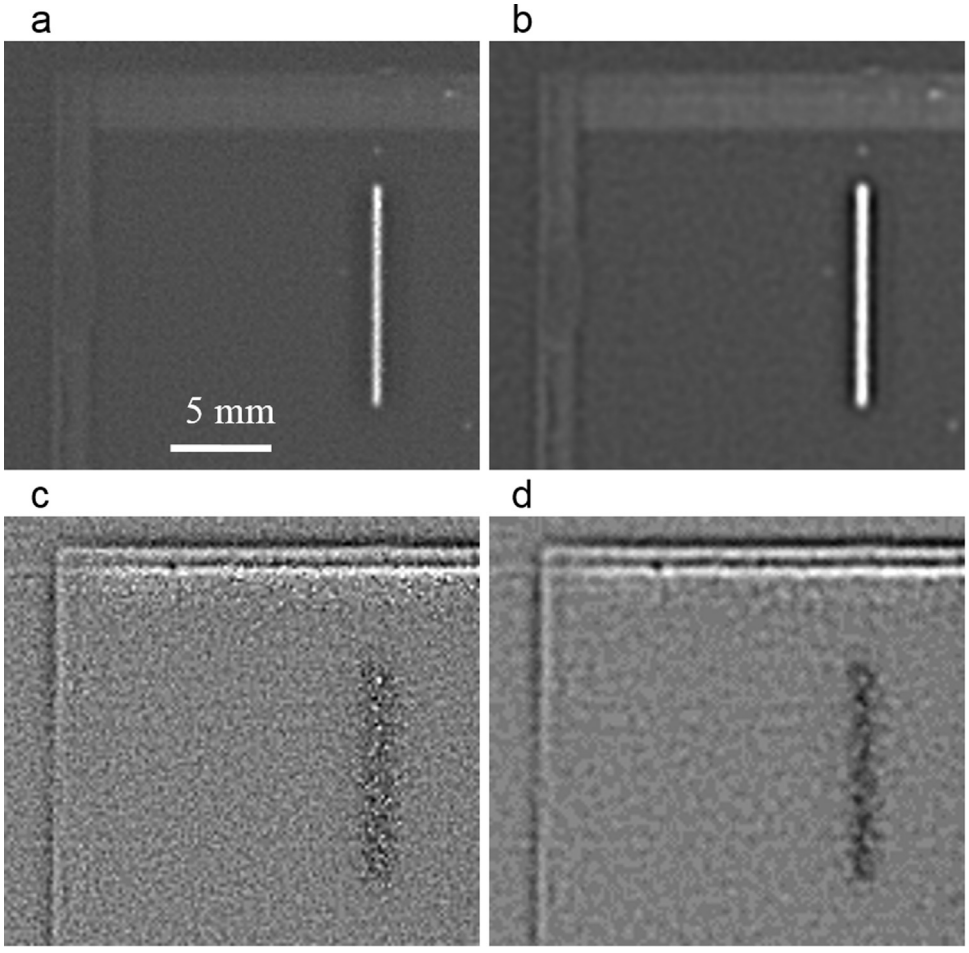

Fig. 7. (a) Power image for sources assumed at the top, (b) power image for sources assumed at the bottom, both scaled from − 30–70 μW/pixel, (c) imaginary image for sources assumed at the top, (d) imaginary image for sources lying at the bottom, both scaled from -10^{-5} to 10^{-5} a.u.

The mean power density in the scratch region of Fig. 7(a) is 62 μW/pixel, which roughly corresponds to the value of 90.9 μW/pixel obtained from the 0° difference signal. Interestingly, images (b) and (d) indicate a stronger blurring than (a) and (c), though for all deconvolutions the same value of $K = 200$ was used. This is probably due to the fact that, for assuming the heat sources to lie at the top, the PSF shows a sharper maximum in the center than for the heat sources lying at the bottom. It must be said that the heat source at the back contact at the top of the images do not clearly show the expected positive imaginary signal in (c). Note that, according to Fig. 7(a) and (b), the power density in this region is significantly lower than at the scratch. Therefore the expected positive imaginary signal in (c) is probably embedded in noise.

5. Discussion

The experimental results shown in the previous section can be taken as a proof of concept of the introduced methods for performing lock-in thermography with depth resolution. The experimental results indicate that the top-minus-bottom method is less disturbed by noise than the imaginary fft signal method. Until now the most convincing result is the 0° top-minus-bottom difference signal, which indeed shows heat sources at the top with positive and sources at the bottom with negative sign and proportional to their power density. In contrast to the phase difference signal, the 0° difference signal is less disturbed by noise and can be evaluated quantitatively. However, the preliminary results of the top-minus-bottom method still show some artifacts. For example, both the phase and the 0° difference images in Fig. 6(c) and (d) still show some residual blurred negative undershoot outside of the scratch. This spurious negative signal is located more at the left side in the upper part of the scratch and more at the right side in its lower part. It was observed in the process of alignment that, if the alignment of the scratch is not perfect, the difference signal shows a strong dark blurred undershoot on one side and a bright blurred overshoot at the other side of the stripe. The observed height-dependence of the remaining blur indicates that here there is a small angular misalignment between the front and the back LIT images. Hence, in a future software used for aligning these two images not only the position but also the angle should be variable. Other reasons for the observed imperfections of the results may be slightly different injection conditions and differences in the emission properties of the top and bottom black layers.

The potential of the imaginary fft signal method of using only one LIT measurement to obtain the same information could not be shown convincingly yet. There is certainly plenty of room for improvement. For example the paint layer can be included in the modeling of the heat transfer using the transfer function formalism [5]. It may also be worthwhile to reduce noise by pixel binning or by using more sophisticated numerical techniques for image deconvolution. It is also possible that the materials data for calculating the PSF are not exactly met or that the full-area back contact layer influences the PSF. There are indications that at least part of the noise in the images used here is not statistical noise but due to noisy gain data of the two-point pixel correction of the IR camera. For further developing the method, a combination of the fft-based deconvolution, e.g. assuming the heat sources to lie in the middle of the depth, leading to the sum of all heat sources, and the 0° front-minus-back method evaluated by the scaling factor

given in Fig. 4(b), leading to vertical height differences, can be imagined. Also the used lock-in frequency and the black layers for increasing the IR emissivity can be further optimized.

The authors like to thank InfraTec GmbH Dresden [11] for providing and further developing the PV-LIT system used for these investigations and J. Bauer (Halle) for stimulating discussions.

References

[1] X.P. Maldague, Theory and Practice of Infrared Vision, 2nd ed., Wiley, New York, 2014.
[2] G. Busse, From photothermal radiometry to lock-in thermography methods, J. Phys: Conf. Ser. 214 (2010) 012003.
[3] O. Breitenstein, W. Warta, M. Langenkamp, Lock-in Thermography, Springer, Berlin, Heidelberg, 2010.
[4] U. Seidel, K. Haupt, H.G. Walther, An attempt towards quantitative photothermal microscopy, J. Appl. Phys. 78 (1995) 2050–2056.
[5] H. Straube, O. Breitenstein, J.-M. Wagner, Thermal wave propagation in thin films on substrate: the time-harmonic thermal transfer function, Phys. Stat. Solidi. B 248 (2011) 2128–2141.
[6] A. Schütt, J. Carstensen, J.-.M. Wagner, H. Föll, Local characterization of co-firing-induced inhomogeneities of conventional mc-Si solar cells, in: Proceedings of the 28th EU PVSEC, Paris, 2013, pp. 1533–1537.
[7] S. Rißland, T.M. Pletzer, H. Windgassen, O. Breitenstein, Local thermographic efficiency analysis of multicrystalline and cast-mono silicon solar cells, IEEE J.-PV 3 (2013) 1192–1199.
[8] F. Ch. Schmidt, Altmann, O. Breitenstein, Application of lock-in thermography for failure analysis in integrated circuits using quantitative phase shift analysis, Mater. Sci. Eng. B 177 (2012) 1261–1267.
[9] See ⟨http://www.maxplanckinnovation.de/en/⟩.
[10] See ⟨www.labir.eu⟩.
[11] See ⟨www.infratec.eu⟩.
[12] See ⟨www.gimp.org⟩.